J. Fluid Mech. (1990), *vol.* 214, *pp.* 455–468
Printed in Great Britain

Unsteady expansion of an ideal gas into a vacuum

By D. M. MOODY
The Aerospace Corporation, Los Angeles, CA 90009, USA

(Received 27 December 1988)

The unsteady expansion of an ideal gas into a vacuum is studied in one-dimensional planar and spherical geometries. The free-molecular expansion of a Maxwell-distributed gas is compared to the continuum expansion of a perfect gas with $\gamma = \frac{5}{3}$. Time histories of density, temperature, and wall pressure (i.e. pressure on a wall surface oriented normal to the flow) are given at four near-field locations, and the approach to far-field behaviour is illustrated. In the free-molecular limit, closed-form expressions for the wall pressure, translational temperature, and fluxes of momentum, kinetic energy, and thermal energy have been obtained in addition to previously published results for density and velocity. The density and dynamic fluxes are observed to decay more rapidly in the tails of continuum pulses than in free-molecular pulses. The reverse is true for wall pressure, which decays less rapidly in continuum flow. Translational temperature, in the free-molecular case, rises discontinuously upon pulse arrival, and, at long times approaches $\frac{2}{3}$ for planar flow and tends to zero for spherical flow. Continuum thermodynamic temperature pulses, on the other hand, rise and fall in simple relation to continuum density. The far-field peak wall pressure in both Knudsen-number limits is found to decrease in inverse (or inverse cubic) proportion to the distance from the initial planar (or spherical) region. This result for the spherical case is at odds with the experiments of Ahrens, Allen & Kovach (1971) which indicate a more rapid ($\xi^{-3.5}$) fall-off of peak overpressure with distance from a point source in a vacuum.

1. Introduction

The one-dimensional expansion of an ideal gas into a vacuum will be investigated in the free-molecular (infinite Knudsen number) and continuum (zero Knudsen number) limits. The gas is assumed to be initially at rest, uniform in temperature and density, and to occupy either the volume interior to a sphere of radius l or the volume between two parallel planes separated by $2l$. Suppose that at time zero the boundary of the initial region is removed. We desire the subsequent time history of density, temperature, and wall pressure at an observation point (field point) external to the initial region. The term 'wall pressure' is used here to mean the pressure exerted on a rigid wall oriented normal to the expanding flow at the field point. The density and temperature, however, are computed for a free field (i.e. no wall).

In the free-molecular limit, it is possible to obtain closed-form expressions for all flow variables of interest. Expressions for density and velocity in both geometries were given by Molmud (1960) and Narasimha (1962). The method formalized by the latter author is used in this paper to additionally evaluate wall pressure, translational temperature, and fluxes of momentum, kinetic energy, and thermal energy.

Exact results from the continuum viewpoint are more difficult to come by,

although an analytical solution for the planar free-field problem appears in the classic monograph by Courant & Friedrichs (1948). Wall pressure following the reflected shock is not treated, however; nor is the spherical problem which is analytically intractable in the continuum regime. Greenspan & Butler (1963) approximate the planar continuum flow field close to a wall for times immediately following shock reflection. The asymptotic behaviour of the flow in both geometries and in both Knudsen-number limits is discussed by Mirels & Mullen (1963), but they do not compare the free-molecular and continuum flows in the near field at early times. The asymptotic continuum solution is also discussed by Greifinger & Cole (1965). In this paper, the continuum equations are numerically integrated via the method of characteristics. This permits complete time behaviour of the near- and far-field continuum flow in both geometries to be compared to the closed-form free-molecular results. The approach of the continuum solution to a far-field limit (defined as the limit in which the pressure gradient vanishes) is also investigated. Comparison of the free-molecular and continuum propagation of the initial density discontinuity in a shock tube was made by Bienkowski (1965).

This study has obvious application to space flight operations, e.g. prediction of the time history of forces produced on spacecraft surfaces as a result of pulsed propellant release. The results are also expected to be of use in providing bounding comparisons for Monte Carlo simulations of unsteady gas expansions into a vacuum.

2. Calculations

For times $t < 0$, an ideal gas is imagined to be confined in one of two initial geometries: either between two planes or within a sphere. With Cartesian axes (x_1, x_2, x_3), let the planar boundaries lie at $x_1 = \pm l$, and let the spherical boundary be centred at the origin and have radius $l = (x_1^2 + x_2^2 + x_3^2)^{\frac{1}{2}}$. In both geometries, a vacuum will be assumed to exist exterior to the gas. The gas within this initial region is assumed to be macroscopically at rest and to be uniform in temperature T_0 and density ρ_0. The gas constant will be denoted by R and the specific heat ratio by γ.

At time $t = 0$, the boundary is removed, and the subsequent gas density, temperature, velocity, and wall pressure are desired as functions of space and time. Time histories of the various quantities of interest for both planar and spherical flows are calculated at four different locations (field points) on the x_1-axis, specifically: $\xi = x_1/l = 2$, 5, 10, and 20. The calculations are made from two diversely limiting viewpoints: the free-molecular and the continuum.

2.1. *The free molecular view*

In this view, the gas molecules are assumed to never collide as they travel from the initial region to the measurement location, i.e. the mean free path is infinite in comparison to any other length in the problem (infinite Knudsen number). The physics of this viewpoint and the analytical technique required for calculating the collisionless flow field have been treated thoroughly by Narasimha (1962). Therein it is shown from the Boltzmann equation, that the distribution function

$$f(\boldsymbol{x}, t; \boldsymbol{v})$$

of molecular velocities $\boldsymbol{v}$ is, in the absence of collisions, preserved on molecular paths

$$\boldsymbol{x} = \boldsymbol{x}' + \boldsymbol{v}t, \tag{1}$$

where x' is the molecular position at $t = 0$. Thus, an initial velocity distribution

$$f(x, 0; v) = f_0(x'; v)$$

remains unaltered at subsequent times ($t > 0$), provided location and time (x, t) are related by (1), i.e.

$$f(x, t; v) = f_0\left(x'; \frac{x - x'}{t}\right).$$

Any macroscopic flow variable $\langle g \rangle$ is then expressed as an expectation value in the distribution f:

$$\langle g(x, t) \rangle = \int g(v) f(x, t; v)\, \mathrm{d}^3 v = \frac{1}{t^3} \int g\left(\frac{x - x'}{t}\right) f_0\left(x'; \frac{x - x'}{t}\right) \mathrm{d}^3 x'. \tag{2}$$

The integral $\int \mathrm{d}^3 x'$ extends over the volume occupied by the gas at $t = 0$, and the Jacobian, t^{-3}, of the transformation arises from (1).

In the results which follow, the molecules are assumed to initially be Maxwell-distributed, i.e.

$$f_0(x'; v) = f_0(v^2) = \left(\frac{\beta_0}{\pi}\right)^{\frac{3}{2}} \mathrm{e}^{-\beta_0 v^2}, \tag{3}$$

where

$$v^2 = \frac{1}{t^2}[(x_1 - x_1')^2 + (x_2 - x_2')^2 + (x_3 - x_3')^2]$$

and

$$\beta_0 = \frac{1}{2RT_0}.$$

As mentioned previously, the measurement location is taken to lie on the x_1-axis, i.e. $x_2 = x_3 = 0$. For the planar and spherical geometries considered, this obviously causes no loss of generality.

2.1.1. *Fundamental quantities*

According to (2), the density is computed as

$$\langle \tilde{\rho} \rangle = \frac{\langle \rho \rangle}{\rho_0} = \frac{1}{t^3} \int f_0\, \mathrm{d}^3 x'. \tag{4}$$

(The tilde is used to denote normalized flow variables.)

The x_1-component of mass flux is

$$\langle \tilde{M}_1 \rangle = \frac{\langle \rho v_1 \rangle}{\rho_0 / \beta_0^{\frac{1}{2}}} = \frac{\beta_0^{\frac{1}{2}}}{t^3} \int v_1 f_0\, \mathrm{d}^3 x' = \frac{\beta_0^{\frac{1}{2}}}{t^3} \int \left(\frac{x_1 - x_1'}{t}\right) f_0\, \mathrm{d}^3 x'. \tag{5}$$

The other two components of mass flux vanish by symmetry.

The x_1-component of momentum flux transported along the x_1-axis is

$$\langle \tilde{P}_{11} \rangle = \frac{\langle \rho v_1^2 \rangle}{p_0} = \frac{\langle \rho v_1^2 \rangle}{\rho_0 / 2\beta_0} = \frac{2\beta_0}{t^3} \int v_1^2 f_0\, \mathrm{d}^3 x', \tag{6}$$

and the sum of the remaining two diagonal elements of the momentum flux tensor is

$$\langle \tilde{P}_{22} + \tilde{P}_{33} \rangle = \frac{\langle \rho v_2^2 + \rho v_3^2 \rangle}{p_0} = \frac{2\beta_0}{t^3} \int (v_2^2 + v_3^2) f_0\, \mathrm{d}^3 x', \tag{7}$$

while all off-diagonal elements, e.g. $\langle \tilde{P}_{12} \rangle$, vanish by symmetry.

The x_1-component of kinetic energy flux is

$$\langle \tilde{K}_1 \rangle = \frac{\langle \frac{1}{2}\rho v^2 v_1 \rangle}{p_0/\beta_0^{\frac{1}{2}}} = \frac{2\beta_0^{\frac{3}{2}}}{t^3} \int \tfrac{1}{2} v^2 v_1 f_0 \, \mathrm{d}^3 x' \tag{8}$$

Again, the x_2- and x_3-components vanish.

2.1.2. *Derived quantities*

Considering the quantities given by (4)–(8) as fundamental, it is possible to derive from them additional flow variables of interest. For example, the x_1-component of flow velocity is

$$\langle \tilde{v}_1 \rangle = \beta_0^{\frac{1}{2}} \langle v_1 \rangle = \langle \tilde{M}_1 \rangle / \langle \tilde{\rho} \rangle. \tag{9}$$

Translational temperature is given by

$$\tfrac{3}{2} R T_{\mathrm{tr}} = \tfrac{1}{2} \langle \boldsymbol{c} \cdot \boldsymbol{c} \rangle,$$

where

$$\boldsymbol{c} = \boldsymbol{v} - \langle \boldsymbol{v} \rangle$$

is the so-called thermal or peculiar velocity. Thus

$$\tfrac{3}{2} R T_{\mathrm{tr}} = \tfrac{1}{2} (\langle v^2 \rangle - \langle \boldsymbol{v} \rangle \cdot \langle \boldsymbol{v} \rangle). \tag{10}$$

Expressing the velocity variance in terms of fundamental quantities, and normalizing with $RT_0 = 1/2\beta_0$ gives

$$\tilde{T}_{\mathrm{tr}} = \frac{T_{\mathrm{tr}}}{T_0} = \frac{2}{3}\left[\frac{1}{2}\frac{\langle \tilde{P}_{11} \rangle + \langle \tilde{P}_{22} + \tilde{P}_{33} \rangle}{\langle \tilde{\rho} \rangle} - \left(\frac{\langle \tilde{M}_1 \rangle}{\langle \tilde{\rho} \rangle}\right)^2\right]. \tag{11}$$

The pressure exerted on a specularly reflecting wall surface which is oriented normal to the flow velocity is equal to twice the normal momentum flux:

$$\langle \tilde{p}_{\mathrm{w}} \rangle = \frac{\langle p_{\mathrm{w}} \rangle}{p_0} = 2 \langle \tilde{P}_{11} \rangle. \tag{12}$$

The x_1-component of thermal energy flux which is associated with the three translational degrees of freedom may be expressed in terms of the fundamental quantities as

$$\frac{\langle \frac{1}{2}\rho \boldsymbol{c} \cdot \boldsymbol{c} v_1 \rangle}{p_0/\beta_0^{\frac{1}{2}}} = \langle \tilde{K}_1 \rangle - \frac{\langle \tilde{M}_1 \rangle}{\langle \tilde{\rho} \rangle}\left(\langle \tilde{P}_{11} \rangle - \frac{\langle \tilde{M}_1 \rangle^2}{\langle \tilde{\rho} \rangle}\right). \tag{13}$$

Finally, if each internal degree of freedom is assumed to transport $\frac{1}{2}RT_{\mathrm{int}}$ of thermal energy, then the total (kinetic plus thermal) energy flux is

$$\langle \tilde{E}_1 \rangle = 2\langle \tilde{K}_1 \rangle - \frac{\langle \tilde{M}_1 \rangle}{\langle \tilde{\rho} \rangle}\left(\langle \tilde{P}_{11} \rangle - \frac{\langle \tilde{M}_1 \rangle^2}{\langle \tilde{\rho} \rangle}\right) + \frac{z-3}{2}\frac{T_{\mathrm{int}}}{T_0}\langle \tilde{M}_1 \rangle. \tag{14}$$

Here z is the total number of molecular degrees of freedom and T_{int} is some 'internal temperature' which is not necessarily equal to the translational temperature (see, for example, Bird 1976).

Narasimha (1962) has given an alternative derivation of higher moments of the distribution function in terms of derivatives of lower moments.

2.1.3. *Evaluation of the quadratures*

Upon evaluation of the integrals in (4)–(8), over the planar initial region, the fundamental quantities for the Maxwell-distributed gas are found to be

$$\langle\tilde{\rho}\rangle = I_1, \quad \langle\tilde{M}_1\rangle = I_2, \quad \langle\tilde{P}_{11}\rangle = I_3 \tag{15a–c}$$

$$\langle\tilde{K}_1\rangle = I_2+I_4, \quad \langle\tilde{P}_{22}+\tilde{P}_{33}\rangle = 2I_1, \tag{15d, e}$$

where

$$I_1 = \tfrac{1}{2}[\mathrm{erf}\,(n)-\mathrm{erf}\,(m)], \quad I_2 = \frac{1}{2\pi^{\frac{1}{2}}}[\mathrm{e}^{-m^2}-\mathrm{e}^{-n^2}], \tag{16a, b}$$

$$I_3 = I_1+\frac{1}{\pi^{\frac{1}{2}}}[m\,\mathrm{e}^{-m^2}-n\,\mathrm{e}^{-n^2}], \quad I_4 = I_2+\frac{1}{2\pi^{\frac{1}{2}}}[m^2\,\mathrm{e}^{-m^2}-n^2\,\mathrm{e}^{-n^2}] \tag{16c, d}$$

and

$$m = (\xi-1)/\tau, \quad n = (\xi+1)/\tau;$$

and the dimensionless position ξ and dimensionless time τ are defined by

$$\xi = x_1/l, \quad \tau = t/l\beta_0^{\frac{1}{2}} \tag{17}$$

For the spherical initial region, the fundamental quantities are found to be

$$\langle\tilde{\rho}\rangle = I_1-L_1, \quad \langle\tilde{M}_1\rangle = I_2-L_2, \quad \langle\tilde{P}_{11}\rangle = I_3-L_3, \tag{18a–c}$$

$$\langle\tilde{K}_1\rangle = I_2+I_4-L_2-L_4, \quad \langle\tilde{P}_{22}+\tilde{P}_{33}\rangle = 2(I_1-L_1-L_5), \tag{18d, e}$$

where the functions $I_i (i = 1,2,3,4)$ are given by (16) and the functions $L_i (i = 1,2,\ldots,5)$ are each of the form:

$$L_i = \frac{1}{\pi^{\frac{1}{2}}}\exp\left[-\left(\frac{\xi^2+1}{\tau^2}\right)\right]\left[\alpha_i \sinh\left(\frac{2\xi}{\tau^2}\right)-\beta_i \cosh\left(\frac{2\xi}{\tau^2}\right)\right], \tag{19}$$

where

$$\alpha_1 = \frac{\tau}{\xi}, \qquad \beta_1 = 0,$$

$$\alpha_2 = 1+\frac{\tau^2}{2\xi^2}, \qquad \beta_2 = \frac{1}{\xi},$$

$$\alpha_3 = \frac{2}{\xi\tau}+\frac{\tau^3}{\xi^3}+\frac{2\tau}{\xi}+\frac{2\xi}{\tau}, \qquad \beta_3 = \frac{4}{\tau}+\frac{2\tau}{\xi^2},$$

$$\alpha_4 = \frac{3}{\tau^2}+\frac{\tau^2}{\xi^2}+\frac{\xi^2}{\tau^2}+\frac{3}{2}+\frac{1}{2\xi^2}, \qquad \beta_4 = \frac{2}{\xi}+\frac{3\xi}{\tau^2}+\frac{1}{\tau^2\xi},$$

$$\alpha_5 = -\frac{\tau^3}{2\xi^3}, \qquad \beta_5 = -\frac{\tau}{\xi^2}.$$

The results (15*a*, *b*) and (18*a*, *b*) were given by Narasimha (1962)†, but the higher moments for momentum flux and kinetic energy flux in (15*c*, *d*, *e*) and (18*c*, *d*, *e*) have apparently not been published previously. The evaluation of the quadratures is straightforward, although cumbersome.

† When (18*a*, *b*) and (19) are substituted into (9), the flow velocity in spherical geometry is found to be

$$\langle\tilde{v}_1\rangle = \frac{1}{\pi^{\frac{1}{2}}\langle\tilde{\rho}\rangle}\sinh\left(\frac{2\xi}{\tau^2}\right)\exp\left(-\frac{\xi^2+1}{\tau^2}\right)\left\{\frac{1}{\xi}\coth\left(\frac{2\xi}{\tau^2}\right)-\frac{\tau^2}{2\xi^2}\right\}.$$

This reveals an error in the last term of Narasimha's (1962) second of equations (3.14).

The axisymmetric unsteady expansion of a monatomic gas into vacuum was analysed via the Boltzmann equation in the limit of small source Knudsen number by Freeman & Grundy (1968). A solution for Maxwellian molecules, valid for large time, was constructed. This asymptotic solution was shown to match the collisionless solution (preservation of the Maxwell distribution) except in the region near the expansion front. The same analysis, applied to the unsteady spherically symmetric expansion, was given by Grundy & Thomas (1969).

The first exact solution of the Boltzmann equation with non-vanishing collision integral was discovered by Krook & Wu (1976), and the existence of additional similarity solutions was investigated by Tenti & Hui (1978). Rather than attempting to incorporate collisions in the Boltzmann equation, let us now abandon the particulate view of the gas altogether and analyse the gas motion in the continuum model.

2.2. *The continuum view*

In this view, the molecular mean free path is vanishingly small in comparison to any other length in the problem (zero Knudsen number). The gas, as it expands, may therefore be assumed to remain at all times a system describable by equilibrium thermodynamics and continuum conservation laws. We then have the problem of rarefaction waves emanating from either two planes or a spherical surface and terminating in a vacuum. As discussed previously, analytical progress is now more difficult, especially for the spherical problem. Therefore, the approach taken here is to obtain the complete time behaviour by numerically integrating the continuum equations via the method of characteristics.

The continuity equation is

$$\frac{\partial \rho}{\partial t}+\frac{1}{x_1^j}\frac{\partial}{\partial x_1}(x_1^j \rho u_1)=0, \tag{20}$$

where $j=0$ or $j=2$ for the planar or spherical problem, respectively. The continuum density is denoted by ρ, and u_1 is the continuum velocity component in the x_1-direction. Conservation of momentum in both geometries is expressed by

$$\frac{\partial u_1}{\partial t}+u_1\frac{\partial u_1}{\partial x_1}+\frac{1}{\rho}\frac{\partial p}{\partial x_1}=0, \tag{21}$$

where p is the continuum pressure. Since the gas expands into a vacuum, shock waves cannot form, and all gradients will decrease with time. The entire flow field is therefore uniform in entropy (homentropic) at all times. Casting the above two equations into characteristic form, (see, for example, Whitham 1974), and using the homentropic ideal-gas state relations to eliminate pressure and density in favour of continuum sound speed gives

$$\left(\frac{\mathrm{d}}{\mathrm{d}\tau}\right)^{\pm} \tilde{J}_{\pm}=\mp\frac{j\tilde{a}\tilde{u}}{\xi} \tag{22}$$

on characteristics

$$\left(\frac{\mathrm{d}\xi}{\mathrm{d}\tau}\right)_{\pm}=\tilde{u}\pm\tilde{a}, \tag{23}$$

where ξ and τ are the dimensionless length and time, defined in (17). The normalized continuum sound speed and flow velocity are

$$\tilde{a}=\beta_6^{\frac{1}{2}}a, \quad \tilde{u}=\beta_6^{\frac{1}{2}}u_1,$$

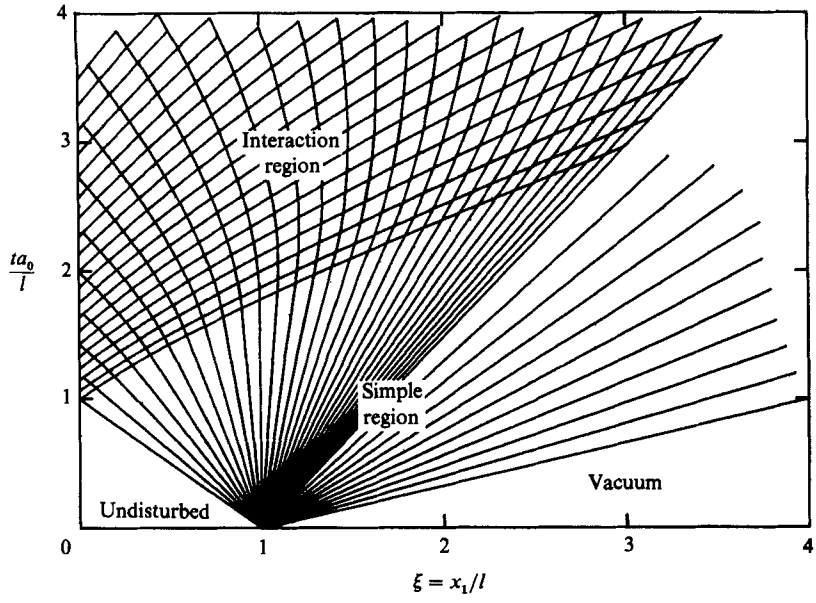

FIGURE 1. Wave diagram for continuum planar flow with $\gamma = \frac{5}{3}$. Expansion propagates with speed a_0 into the undisturbed region and terminates in a vacuum along $x_1 = l + 2a_0 t/(\gamma - 1)$.

the characteristic operators are

$$\left(\frac{\mathrm{d}}{\mathrm{d}\tau}\right)^{\pm} = \frac{\partial}{\partial\tau} + (\tilde{u} \pm \tilde{a})\frac{\partial}{\partial\xi},$$

and the Riemann variables are

$$\tilde{J}_{\pm} = \tilde{u} \pm \frac{2\tilde{a}}{\gamma - 1}.$$

The characteristics for the planar problem with $\gamma = \frac{5}{3}$ are shown schematically on the wave diagram in figure 1. (The actual computational mesh was much more dense.) The front of the expansion wave propagates from the boundary at $\xi = 1$ into the undisturbed region at the sound speed a_0 in that region. The wave terminates in vacuum along the characteristic

$$\xi = 1 + \frac{2}{\gamma - 1}\frac{a_0 t}{l}$$

which, as discussed by Greenspan & Butler (1963), is also the terminating characteristic for the spherical problem. The indicated simple region is affected only by the expansion which originates from $\xi = 1$, while the interaction region is influenced by the expansions from both $\xi = 1$ and $\xi = -1$.

After integrating (22) along the characteristics to obtain the fundamental variables $\tilde{u}$ and $\tilde{a}$, all other quantities of interest are easily determined. The continuum density and temperature (cf. (4) and (11)) follow from the homentropic relations:

$$\tilde{\rho} = \frac{\rho}{\rho_0} = \left[\left(\frac{2}{\gamma}\right)^{\frac{1}{2}}\tilde{a}\right]^{2/(\gamma-1)}, \tag{24}$$

$$\tilde{T} = \frac{T}{T_0} = \frac{2}{\gamma}\tilde{a}^2. \tag{25}$$

The normalized fluxes of mass, momentum, and energy are

$$\tilde{M}_1 = \frac{\rho u_1}{\rho_0/\beta_0^{\frac{1}{3}}} = \tilde{\rho}\tilde{u}, \tag{26}$$

$$\tilde{P}_{11} = \frac{\rho u_1^2}{p_0} = 2\tilde{\rho}\tilde{u}^2, \tag{27}$$

$$\tilde{E}_1 = \frac{(e+\frac{1}{2}u_1^2)\rho u_1}{p_0/\beta_0^{\frac{1}{3}}} = \tilde{K}_1 + \frac{2}{\gamma(\gamma-1)}\tilde{\rho}\tilde{a}^2\tilde{u}, \tag{28}$$

where e is the specific internal energy of the gas. These flux expressions are the continuum counterparts of (5), (6), and (14).

If a wall is placed normal to the expanding flow, a shock wave will reflect from it. The shock propagates against the flow and brings it to rest. With the unshocked homentropic flow determined by the method of characteristics, the shocked flow is determined by ideal-gas shock jump conditions. Since the shock wave propagates into a non-uniform field, its velocity continuously changes, and its distance from the wall is therefore computed numerically by a simple first-order time integral of its instantaneous velocity. Conditions at the wall (x_1) are then related to those immediately following the shock (at x_s) by a time delay of $\Delta t = (x_1 - x_s)/a_2$, where a_2 is the shocked sound speed. Specifically, the wall pressure is given by

$$\tilde{p}_w(x_1, t) = \frac{p_w}{p_0} = \tilde{\rho}^\gamma + \tilde{P}_{11}\left(1 + \frac{c_s}{u_1}\right), \tag{29}$$

where the quantities on the right-hand side of the above equation are unshocked values at shock position x_s and time $t - \Delta t$. The shock wave speed c_s (measured relative to the wall) is given by

$$\frac{c_s}{u_1} = \frac{3-\gamma}{4}\left\{\left[\left(\frac{4}{3-\gamma}\right)^2\left[\left(\frac{a}{u_1}\right)^2 + \frac{\gamma-1}{2}\right] + 1\right]^{\frac{1}{2}} - 1\right\}. \tag{30}$$

In the above equation, the Mach number of the unshocked flow may be equivalently expressed as

$$\frac{u_1}{a} = \left(\frac{\tilde{P}_{11}}{\gamma\tilde{\rho}^\gamma}\right)^{\frac{1}{2}}.$$

The wall pressure given by (29) will be compared to the free-molecular pressure given by (12).

3. Comparisons

Results of the continuum calculations for $\gamma = \frac{5}{3}$ are now compared to the free-molecular results for the Maxwell-distributed gas.

Figure 2 shows density time history in the two limits (see (4) and (24)). Note that the results are plotted against $\tau/\xi = t/(x_1\beta_0^{\frac{1}{3}})$ rather than $\tau = t/(l\beta_0^{\frac{1}{3}})$. Displayed in this way, one sees from figure 2(*b*) that the peak density in spherical flow occurs at $\tau/\xi \approx 0.8$ for all four values of ξ. Also, the shapes of the pulses are similar when plotted in this way. This is expected since, in the limit $\xi = x_1/l \to \infty$, the only length with which to non-dimensionalize time is x_1. In this far-field limit then, the flow must depend on the ratio t/x_1, not on t and x_1 individually; i.e. the flow becomes self-

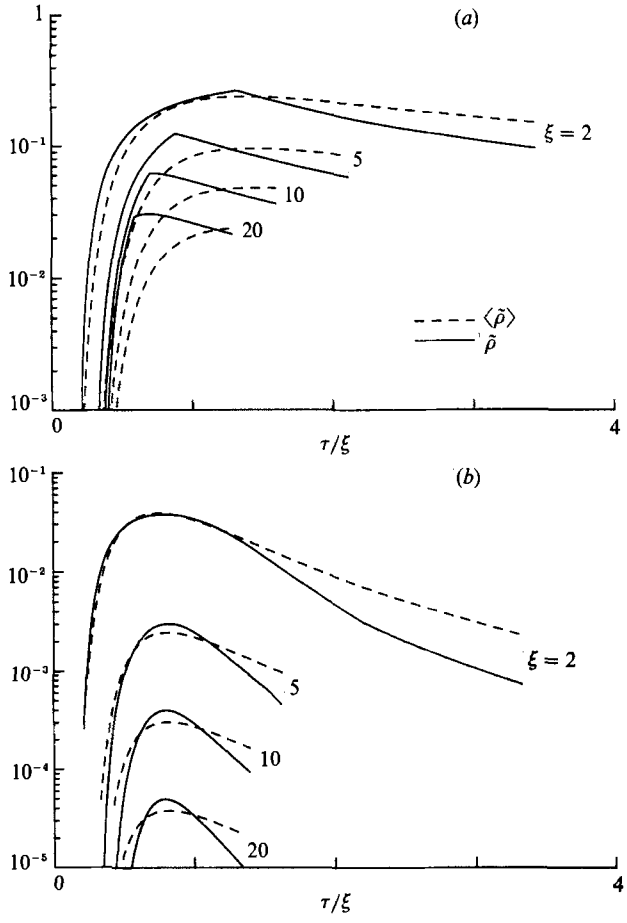

FIGURE 2. Density time history at $\xi = 2$, 5, 10, and 20 for (*a*) one-dimensional planar and (*b*) spherical flow. The free-molecular limit is shown by dashed lines, and the solid lines represent the continuum limit with $\gamma = \frac{5}{3}$.

similar (see, for example, Sedov 1959 or Zel'dovich & Raizer 1966). Figure 2(*a*) shows that the planar free-molecular flow is also self-similar for the displayed range of ξ from 2 to 20, but that the planar continuum flow has not yet attained this nature.

An additional insight into the asymptotic approach of the continuum solution to a far-field limit is gained by noting that the pressure gradient in the momentum equation (21) vanishes in this limit. This being the case, integration of the equation in this limit implies

$$u_1 \to x_1/t \quad \text{as} \quad x_1 \to \infty$$

so long as x_1/t is held constant. Normalizing with a_0 and l, one may write the above as

$$u_1/a_0 \to \eta \quad \text{as} \quad \xi = x_1/l \to \infty,$$

where $\eta = x_1/a_0 t$ is held constant as ξ increases. Or, equivalently

$$\phi(\xi; \eta = \text{const}) \to 0 \quad \text{as} \quad \xi \to \infty,$$

where

$$\phi(\xi; \eta) \equiv \frac{u_1(\xi; \eta)}{a_0 \eta} - 1.$$

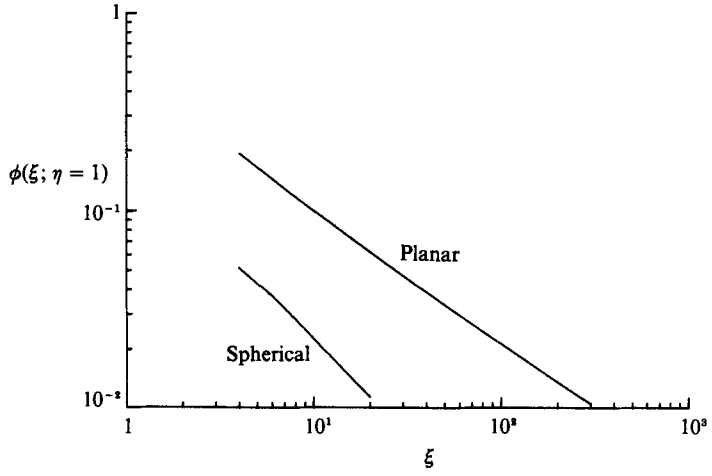

FIGURE 3. Asymptotic approach of the continuum solution to the far-field limit. As ϕ vanishes, the flow at $\eta = x_1/a_0 t = 1$ attains a limiting velocity of a_0.

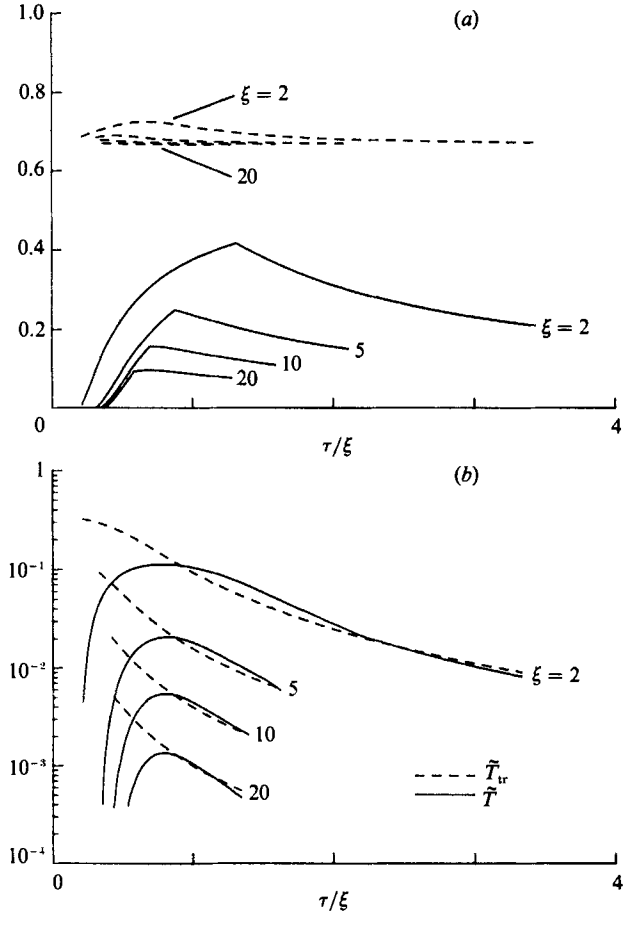

FIGURE 4. Temperature time history at $\xi = 2$, 5, 10, and 20 for (a) one-dimensional planar and (b) spherical flow. The free-molecular limit is shown by dashed lines, and the solid lines represent the continuum limit with $\gamma = \frac{5}{3}$.

The behaviour of $\phi(\xi;\eta=1)$ is shown in figure 3. This function should vanish in the far-field. In spherical flow, $\phi = 0.05$ at $\xi = 4$, but for planar flow ϕ does not decrease to this level until $\xi = 30$. Likewise, ϕ decreases to 0.01 at $\xi = 20$ for the spherical case, in contrast to $\xi \approx 300$ for the planar geometry. Approach to far-field behaviour is thus seen to be much more rapid in spherical flow than it is in planar flow.

The continuum density time history in plane geometry (figure 2*a*) shows a distinct slope discontinuity at roughly $\tau/\xi = 1$. This point marks the arrival of the expansion wave from $\xi = -1$; i.e. this is the end of the simple region and the beginning of the wave interaction region (see figure 1). The free-molecular density, of course, shows no such wave-like behaviour. In both geometries, it is apparent that the density decays more rapidly in the tail of the continuum pulse than it does in the free-molecular pulse. The pulse shapes are, however, qualitatively similar in both flow regimes.

Figure 4 shows temperature time history in the two limits (see (11) and (25)). These comparisons point out a fundamental difference between the two flow regimes.

In the microscopic, free-molecular viewpoint, the translational temperature $\tilde{T}_{\rm tr}$ is essentially a measure of the variance of the molecular velocity distribution (see (10)). Thus, $\tilde{T}_{\rm tr}$ jumps discontinuously upon the arrival of any number of molecules, however small, provided they are distributed in velocity (see figure 4). For large values of τ/ξ, the translational temperature tends to $\frac{2}{3}$ for planar flow and to zero for spherical flow. These tendencies are explained as follows. At long times, we are selecting only the very slowest molecules in the x_1-component of velocity from the Maxwell distribution. However, the *transverse* velocity components in the planar case are totally unrestricted. The full spectrum of x_2- and x_3-component velocities are observed at all times since the initial region is of infinite extent in those directions. That is, carriers of very large transverse velocity came from initial positions which were very distant from the x_1-axis, and those with small transverse velocity came from positions close to the x_1-axis. Although the mean of each transverse velocity component vanishes, the mean square does not, and each mean square contributes $\frac{1}{3}$ to the translational temperature. In spherical geometry, selection of slowly travelling molecules in the x_1-direction simultaneously limits the spectrum of transverse velocities that will be observed. This is due to the finite extent of the initial region. Those carriers arriving with the largest transverse velocities came from initial positions that were only one sphere radius l distant from the x_1-axis. At large distances, where the spherical initial region may be considered a point source, only one velocity class may reach the field point at any given time. In this limit then, the variance (and thus the translational temperature) vanishes.

In contrast to free-molecular flow, continuum temperature in the homentropic flow of an ideal gas is purely a function of density (equation (25)). Thus, for example, the maxima in continuum temperature (see figure 4) coincide with the maxima in continuum density (figure 2) and $\tilde{T} \to 0$ as $\tilde{\rho} \to 0$.

In summary, translational temperature in the free-molecular model is related to an underlying microscopic motion of gas molecules. By contrast, thermodynamic temperature in the continuum model is a variable of state, defined in general as a function of three other state variables: internal energy, entropy, and density:

$$T = \left(\frac{\partial e}{\partial s}\right)_{\rho}.$$

This definition does not explicitly involve the macroscopic flow velocity, u_1. Furthermore, in the continuum flows considered here, the gas is calorically perfect

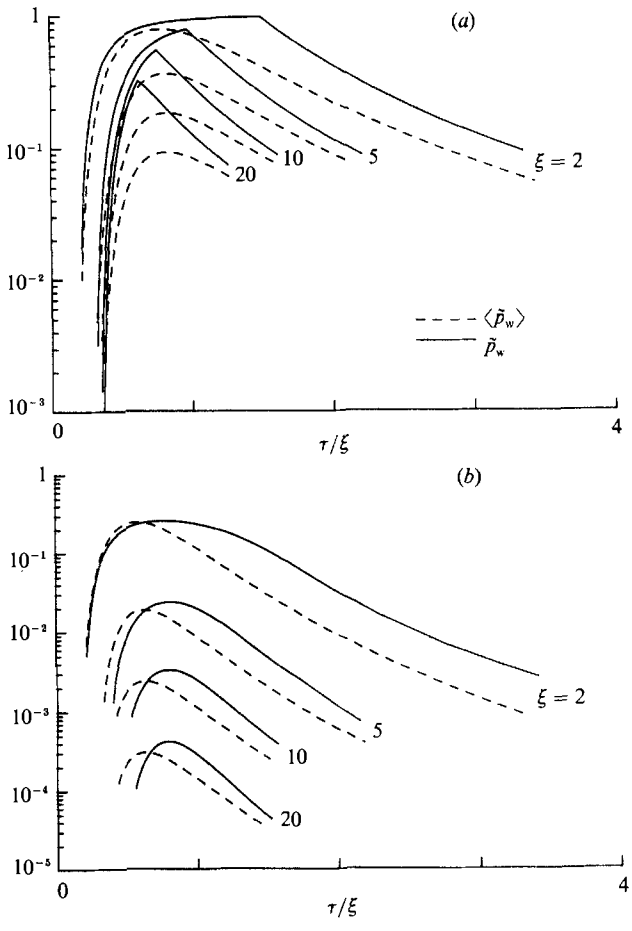

FIGURE 5. Wall pressure time history at $\xi = 2$, 5, 10, and 20 for (*a*) one-dimensional planar and (*b*) spherical flow. The free-molecular limit is shown by dashed lines, and the solid lines represent the continuum limit with $\gamma = \frac{5}{3}$.

and homentropic. The thermodynamic temperature thus reduces to a function of density alone.

Although not shown, the time histories of the fluxes of mass, momentum, and energy have the same qualitative appearance as the density itself (figure 2).

Figure 5 compares the free-molecular wall pressure $\langle \tilde{p}_w \rangle$ given in (12) with the continuum wall pressure $\tilde{p}_w$ of (29). Generally speaking, the continuum peaks are higher and occur later than the free-molecular peaks. Also, there is a less rapid decay in the tail of the continuum pulse than in the free-molecular pulse. This is opposite to the behaviour of the density pulses.

In the far field (say $\xi > 20$), the following scaling relations for the planar free-molecular flow are numerically deduced:

$$\langle \tilde{p}_{max} \rangle = 1.85\xi^{-1} \quad \text{at} \quad (\tau/\xi)_{max} = 0.82$$

and

$$\langle \tilde{I} \rangle = 2.26,$$

where $\langle \tilde{p}_{max} \rangle$ is the peak wall pressure, $(\tau/\xi)_{max}$ is its time of occurrence, and $\langle \tilde{I} \rangle$ is

the impulse (time integral) of the pressure. Similarly, for the spherical free-molecular flow

$$\langle \tilde{p}_{\max} \rangle = 2.44\xi^{-3} \quad \text{at} \quad (\tau/\xi)_{\max} = 0.63$$

and

$$\langle \tilde{I} \rangle = 1.50\xi^{-2}.$$

In the continuum limit, the same peak pressure versus distance relations prevail in the far field; i.e. $\tilde{p}_{\max} \sim \xi^{-(j+1)}$ for the planar ($j = 0$) and spherical ($j = 2$) cases. This may be deduced from (29) and the fact that, in the far field, the velocity u_1 approaches the limit of x_1/t. The Mach number therefore grows infinitely large as the density and thus sound speed vanish. The ratio c_s/u_1 therefore approaches a limiting constant value which depends only on γ (see (30)). The wall pressure thus depends on density as

$$\tilde{p}_w \sim \tilde{\rho}^{\gamma} + \text{const}\,\tilde{\rho}.$$

Since $\gamma > 1$, and the density decreases in inverse (or inverse cubic) proportion to distance for the planar (or spherical) expansion, it follows that

$$\tilde{p}_{\max} \sim \xi^{-(j+1)}$$

represents the dominant far-field behaviour of the peak wall pressure.

The wall pressure $\tilde{p}_w$ is the quantity of most immediate interest in application. It is also the quantity which is most readily measurable by experiment.

In the experiments of Ahrens, Allen & Kovach (1971), high-explosive pellets were detonated in a vacuum tank, and peak wall pressures were found to decrease as $\xi^{-3.5}$ rather than as ξ^{-3}. There are several possible reasons for the disagreement between these experiments and the current calculations. In the first place, the gas cloud of products following the detonation of the solid phase explosive certainly does not have the same simple uniform initial conditions as considered in this paper. Secondly, and most importantly, the measurements were made at distances ranging from 28 to 409 solid-phase radii. It is not clear that this range lay in the far field of the gas phase. As discussed above, the inverse cubic fall-off of peak pressure with distance is only dominant at distances so large that the flow velocity has reached its vacuum-limiting value. Finally, if the measurements were in the gas near field, non-ideal behaviour of the products and radiation could help to explain the more rapid fall-off. Apparently, no data exist for the theoretically simpler problem considered in this paper.

4. Summary

The planar and spherical one-dimensional unsteady expansion of an ideal gas into a vacuum has been studied in the free-molecular and continuum limiting viewpoints. Complete time behaviour of density, temperature, and wall pressure, in both Knudsen-number limits has been given at four near-field locations, and the approach of the continuum flow to far-field behaviour has been illustrated.

Density and dynamic fluxes are observed to decay more rapidly in the tails of continuum pulses than in free-molecular pulses. The reverse is true for wall pressure, which decays less rapidly in continuum flow. Translational temperature in the free-molecular case jumps discontinuously at the leading edge of the pulse and then tends asymptotically in time to either $\frac{2}{3}$ or zero for the planar or spherical expansion, respectively. Continuum temperature, on the other hand, is related simply to density.

Closed-form expressions for free-molecular wall pressure, translational tem-

perature, and fluxes of momentum and energy have been obtained in addition to previously published results for density and mass flux.

Peak wall pressure in both Knudsen-number limits is found, in the far-field limit, to decrease in inverse (or inverse cubic) proportion to the distance from the initial planar (or spherical) region. This is at odds with the experiments of Ahrens *et al.* (1971) which indicate a more rapid ($\xi^{-3.5}$ as opposed to ξ^{-3}) fall-off of peak overpressure with distance from a high-explosive pellet in vacuum. The reasons for this difference most likely stem from non-uniform gas initial conditions, and the measurements having been made in the near field of the gaseous detonation products.

Finally, the results presented here are expected to be of use in providing bounding comparisons for Monte Carlo simulations of unsteady gas expansions into vacuum.

The author thanks Dr R. L. Baker for many helpful discussions. This work was supported by the Space Division, US Air Force Systems Command under Contract no. F04701-87-C-0088.

REFERENCES

Ahrens, T. J., Allen, C. F. & Kovach, R. L. 1971 Explosive gas blast: the expansion of detonation products in vacuum. *J. Appl. Phys.* **42**, 815–829.

Bienkowski, G. 1965 Propagation of an initial density discontinuity. In *Rarefied Gas Dynamics*, Vol. I (ed. J. H. DeLeeuw). Academic.

Bird, G. A. 1976 *Molecular Gas Dynamics*. Clarendon.

Courant, R. & Friedrichs, K. O. 1948 *Supersonic Flow and Shock Waves*. Interscience.

Freeman, N. C. & Grundy, R. E. 1968 On the solution of the Boltzmann equation for an unsteady cylindrical symmetric expansion of a monatomic gas into vacuum. *J. Fluid Mech.* **31**, 723–736.

Greenspan, H. P. & Butler, D. S. 1963 On the expansion of a gas into vacuum. *J. Fluid Mech.* **13**, 101–119.

Greifinger, C. & Cole, J. D. 1965 Expansion of a finite mass of gas into vacuum. *AIAA J.* **3**, 1200–1201.

Grundy, R. E. & Thomas, D. R. 1969 Unsteady spherically symmetric expansion of a fixed mass of gas into vacuum. *AIAA J.* **7**, 967–969.

Krook, M. & Wu, T. T. 1976 Formation of Maxwellian tails. *Phys. Rev. Lett.* **36**, 1107–1109.

Mirels, H. & Mullen, J. F. 1963 Expansion of gas clouds and hypersonic jets bounded by a vacuum. *AIAA J.* **1**, 596–602.

Molmud, P. 1960 Expansion of a rarefied gas cloud into vacuum. *Phys. Fluids* **3**, 362–366.

Narasimha, R. 1962 Collisionless expansion of gases into vacuum. *J. Fluid Mech.* **12**, 294–308.

Sedov, L. I. 1959 *Similarity and Dimensional Methods in Mechanics*. Academic.

Tenti, G. & Hui, W. H. 1978 Some classes of exact solutions of the nonlinear Boltzmann equation. *J. Math. Phys.* **19**, 774–779.

Whitham, G. B. 1974 *Linear and Nonlinear Waves*. John Wiley & Sons.

Zel'dovich, Y. B. & Raizer, Y. P. 1966 *Physics of Shock Waves and High-Temperature Hydrodynamic Phenomena*. Academic.